

# No-Switching Quantum Key Distribution using Broadband Modulated Coherent Light

Andrew M. Lance,<sup>1</sup> Thomas Symul,<sup>1</sup> Vikram Sharma,<sup>1</sup> Christian Weedbrook,<sup>1,2</sup> Timothy C. Ralph,<sup>2</sup> and Ping Koy Lam<sup>1</sup>

<sup>1</sup>*Quantum Optics Group, Department of Physics, Faculty of Science, Australian National University, ACT 0200, Australia*

<sup>2</sup>*Department of Physics, University of Queensland, St Lucia, Queensland 4072, Australia*

(Dated: February 9, 2020)

We realize an end-to-end no-switching quantum key distribution protocol using continuous-wave coherent light. We encode weak broadband Gaussian modulations onto the amplitude and phase quadratures of light beams at the Shannon's information limit. Our no-switching protocol achieves high secret key rate via a post-selection protocol that utilizes both quadrature information simultaneously. We establish a secret key rate of 25 Mbits/s for a lossless channel and 1 kbit/s, per 17 MHz of detected bandwidth, for 90% channel loss. Since our scheme is truly broadband, it can potentially deliver orders of magnitude higher key rates by extending the encoding bandwidth with higher-end telecommunication technology.

Quantum key distribution (QKD) [1] is a technique for generating a shared cryptographic key between two parties, Alice and Bob, where the security of the shared key is guaranteed by the laws of quantum mechanics. QKD based on continuous variables [2], promises significantly higher secret key rates in comparison to single photon schemes [1, 3]. Coherent state QKD protocols [4, 5, 6, 7, 8, 9] are the most promising of these continuous variable protocols. They are relatively simple to implement, in contrast to QKD protocols employing "non-classical" states [10]. Coherent states can be readily produced by a well stabilized laser and can be detected using high quantum efficiency detectors. Confidence in the practicability of coherent state QKD protocols has increased since it was shown that the security of these protocols can be ensured for transmission losses greater than 50% using post-selection [6] or reverse reconciliation [7] procedures. In principle, it is therefore possible to generate a secure key even in the presence of arbitrarily high loss. This development, coupled with potentially high secret key rates, render coherent state QKD protocols viable contenders for real-world cryptographic applications.

Our coherent state QKD protocol builds on previous protocols presented in [5, 6, 7] and is an advance on random switching by simultaneously measuring both measurement bases [8]. The QKD protocol operates as follows. Alice prepares a coherent state  $|x_A + ip_A\rangle$  and sends it to Bob. As a result of transmission losses in the quantum channel, vacuum noise is coupled into the transmitted state. On receiving the state, Bob simultaneously measures both the amplitude ( $x$ ) and phase ( $p$ ) quadratures of the state via a 50/50 beam splitter.

The coherent state QKD set-up is shown in Fig. 1. In our implementation we use a bright, continuous-wave, coherent laser operating at 1064 nm. In contrast to pulsed or temporal encoding schemes, we achieve high secret key rates by exploiting the continuous-wave nature of the laser field to implement a true broadband encoding protocol. Our broadband encoding technique uses standard electro-optic modulators to encode weak broadband modulations onto the quantum states at the sideband frequencies of the electromagnetic field. Using this technique, the transmission rate of coherent states can be arbitrarily increased and is only limited by Alice's encoding and Bob's detection bandwidths.

To maximize Bob's detection bandwidth, we simultaneously measure both the amplitude and phase quadratures of the electromagnetic field at Bob's station, using the no-switching protocol [8]. This protocol has a significantly improved secret key rate when compared with previous protocols that rely on random switching between measurement bases. Random switching requires the precise and rapid control of the optical phase of a local oscillator field, which is difficult to achieve in practice. Experimentally, this is implemented using electro-optic phase modulators or Pockel cells, however, these devices have limited operational bandwidths that constrain the switching rate of such systems.

In our experimental implementation using broadband encoding techniques, we only process quantum states encoded on 17 MHz of the sideband frequency spectrum (Fig. 2 (inset)). As intrinsic classical noise is manifest at low frequencies on the laser beam and our data acquisition system has a maximum sample rate of 50 MHz, we process data from frequencies between 33 MHz and 50 MHz with respect to the laser carrier frequency. We verify that the laser field is coherent in this range, finding both the amplitude and phase quadrature variances equal to  $V(x), V(p) = 1.01 \pm 0.01$ , normalized to the quantum noise limit. We digitally filter the data in the identified frequency band and demodulate and re-sample it at 17 MHz. To improve the statistical correlations between Alice's and Bob's data, we apply a previously characterized transfer function to the data, which corrects for the frequency response of Alice's electro-optic modulator and Bob's detectors. After this data processing, Alice and Bob have correlated random data with Gaussian probability distributions, which are represented in a scatter-plot diagram of Alice's and Bob's data (Fig. 2(a)). Using a random subset of this data they can quantify the quantum channel transmission efficiencies of each quadrature ( $\eta_x$  and  $\eta_p$ ), and the variances of Alice's quadrature displacements ( $V(x_A)$  and  $V(p_A)$ ). From these transmission efficiency and variance statistics, Alice and Bob can determine the maximum information an eavesdropper (Eve) could have obtained during quantum state transmission.

Eve's best strategy in our setup where all states are coherent, is to use a beam splitting attack [5, 6], where she replaces the lossy quantum channel with a perfect lossless line and

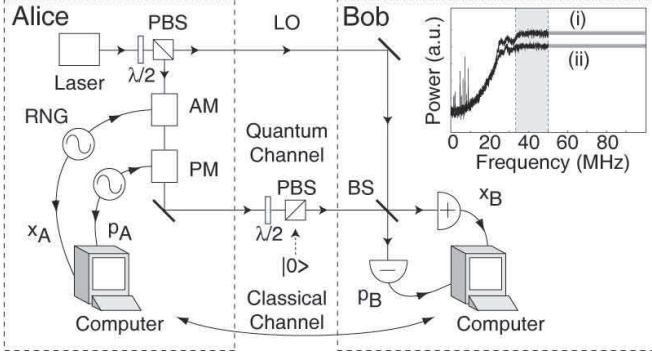


FIG. 1: Schematic of our no-switching coherent state quantum key distribution protocol. LO: local oscillator; RNG: random number generators; AM (PM); amplitude (phase) electro-optic modulators; PBS: polarizing beam splitter;  $\lambda/2$ : half wave plate; BS: 50/50 beam splitter;  $|0\rangle$ : vacuum state,  $x_B$  and  $p_B$ ; Bob's quadrature measurements. (inset) (i) Bob's detected noise spectra of Alice's broadband modulation encoding, (ii) shown with respect to the quantum noise limit. Grey region denotes the 17 MHz region of the sideband frequency spectrum (between 33 MHz and 50 MHz) used in our analysis.

uses a beam splitter to simulate the channel losses. Since Eve is aware that Bob is using the no-switching protocol, Eve's optimum strategy is to simultaneously measuring both the  $x$  and  $p$  quadratures of her resulting ancilla state. We express Eve's information in terms of conditional variances [11] (or uncertainties) of the coherent quadrature displacements of Alice's initial state. Eve's conditional variances are expressed as  $V(x_E|x_A)$  and  $V(p_E|p_A)$ . We show Eve's attack to be optimal by considering that the maximum information that Bob and Eve can simultaneously know about Alice's state is bounded by the Heisenberg-type uncertainty relations [7]  $V(x_B|x_A) \times V(p_E|p_A) \geq 1$  and  $V(p_B|p_A) \times V(x_E|x_A) \geq 1$ . In our QKD protocol, Bob's conditional variances are limited by the quantum noise statistics of a coherent state and can be expressed as  $V(x_B|x_A) = 1$  and  $V(p_B|p_A) = 1$ . Substituting Bob's conditional variances into Eve's uncertainty relations, her minimum conditional variances are bounded by

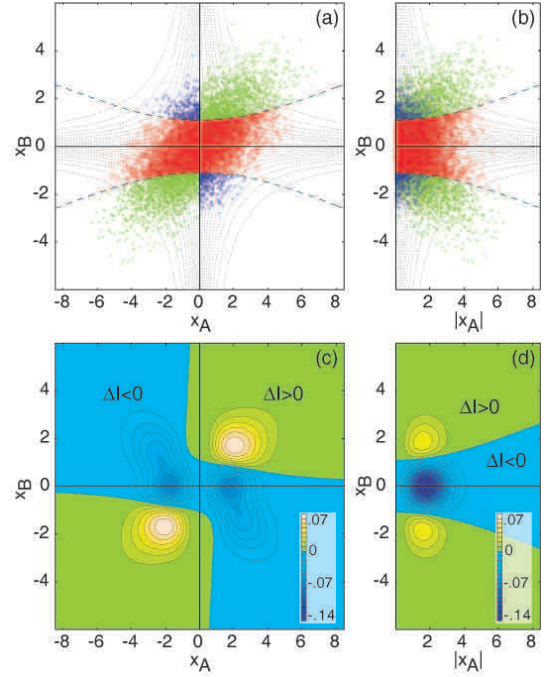


FIG. 2: (a) The “global” perspective of Alice's ( $x_A$ ) and Bob's ( $x_B$ ) data, represented in a scatter-plot diagram, for transmission losses of 54%. Dotted lines: “banded information channels”; Green points: data that has error free binary encoding; Blue points: data that has bit-flip errors; Red points: data that has a negative net information rate. (b) Bob's perspective of his and Alice's data. Bob post-selects data with positive information rates, discarding the red points. (c) A global perspective of the theoretical net information rate contour plots for Alice's and Bob's data. (d) Bob's perspective of the theoretical net information rate contour plots.

the inequalities  $V(p_E|p_A)_{\min} \geq 1$  and  $V(x_E|x_A)_{\min} \geq 1$ . For Eve's optimal attack, her conditional variances are given by  $V(x_E|x_A) = 1$  and  $V(p_E|p_A) = 1$ , thereby saturating the above inequalities and proving that this is the maximal amount of information Eve can access without being revealed.

The security our experiment relies on the indistinguishability of non-orthogonal pure states [12]. For every transmitted state, Alice publicly announces the absolute values  $|x_A|$  and  $|p_A|$ , thereby requiring Bob (and Eve) to distinguish the state from one of the four possible coherent states  $|\pm x_A \pm ip_A\rangle$ . The general solution for the maximum accessible information of four pure states is not known, however, in the case of our experiment where Eve performs an optimal attack, she effectively has to simultaneously distinguish between two non-orthogonal pure states for each quadrature,  $|x_A\rangle$  and  $|-x_A\rangle$  or  $|ip_A\rangle$  and  $|-ip_A\rangle$ . In this case, the maximum accessible

information obtainable is known [13] and is given by

$$I_{AE} = \sum_{v=\{x,p\}} \left[ \frac{1}{2} (1 + \sqrt{1-z_v^2}) \log_2 (1 + \sqrt{1-z_v^2}) \right. \\ \left. + \frac{1}{2} (1 - \sqrt{1-z_v^2}) \log_2 (1 - \sqrt{1-z_v^2}) \right] \quad (1)$$

where  $z_v = |\langle -v_E | v_E \rangle|^2 = e^{-2|v_E|^2} = e^{-(1-\eta_v)|v_A|^2}$  are Eve's quadrature overlap functions, and  $v = \{x, p\}$ .

We calculate Bob's mutual information with Alice [14] using scatter-plot diagrams of Alice's and Bob's state measurements. The "global" perspective of Alice's and Bob's results is shown in Fig. 2(a), whilst Bob's perspective during the QKD protocol (after Alice publicly announces the absolute values of her data) is shown in Fig. 2(b). To interpret information encoded onto the quantum states, Alice and Bob use a binary encoding system based on the directional displacements of the quadrature measurements, interpreting positive displacements in phase space as a binary "1" and negative displacements as a binary "0". Hence two bits of information are encoded per transmitted state (one bit on each quadrature). From the global perspective of Alice's and Bob's results (Fig. 2(a)), the points in the diagonal quadrants correspond to error-free bits, whilst the points in the off-diagonal quadrants correspond to bit-flip errors. We encode at approximately the Shannon capacity of the quantum channel [14] by partitioning Alice's and Bob's data into "banded information channels" (BICs). We achieve this by calculating the theoretical probability of error for Alice's and Bob's data

$$P_v = (e^{-4|v_A v_B| \sqrt{2\eta_v}}) / (1 + e^{-4|v_A v_B| \sqrt{2\eta_v}}) \quad (2)$$

and allocate the data into BICs with increasing probabilities of error, as shown by the dotted hyperbolas in Fig. 2(a) and 2(b). For each BIC, let the number of error-free points be denoted by  $N_{\text{good}}$  and the number of bit-flip errors by  $N_{\text{error}}$ . We calculate the experimental probability of error for each BIC using  $P_v = N_{\text{error}} / (N_{\text{error}} + N_{\text{good}})$ . Bob's mutual information with Alice summed over  $n$  BICs is given by

$$I_{AB} = \sum_{v=\{x,p\}} \sum_{k=1}^n \left[ 1 + P_{(v,k)} \log_2 (P_{(v,k)}) \right. \\ \left. + (1 - P_{(v,k)}) \log_2 (1 - P_{(v,k)}) \right] \quad (3)$$

where  $P_{(v,k)}$  is the probability error rate for the  $k$ th BIC, of either the amplitude or phase quadrature. The mutual information rate between Alice and Bob (Eq. (3)) approaches the Shannon capacity [14] as the number of BICs is increased. In our analysis we partition the data into 10 BICs by assigning an equal number of data points to each, thereby achieving a mutual information rate of  $\sim 99\%$  of the Shannon information limit (Fig. 3 (inset)).

From Bob's perspective, he can calculate the amount of mutual information he has with Alice (Eq. (3)), and Eve has with Alice (Eq. (1)), for each BIC. The total secret information rate summed over all BICs can be expressed as

$$\Delta I = \sum_{v=\{x,p\}} \sum_{k=1}^n \left( I_{AB(v,k)} - \int \int_{S(v,k)} I_{AE} \times P(v_A, v_B) dv_A dv_B \right) \quad (4)$$

where the joint probability distribution of Alice and Bob's measurements is given by  $P(v_A, v_B)$ ,  $S_{(v,k)}$  is the area of the  $k$ th BIC of either the amplitude or phase quadrature, and Bob's mutual information with Alice for the  $k$ th BIC for each quadrature is denoted by  $I_{AB(v,k)}$ . Figure 2(c) is a contour plot of the theoretical net information rate from a "global" perspective of Alice's and Bob's results. Alice and Bob cannot directly use Fig. 2(c), as Bob only knows the absolute values of Alice's data. Bob's perspective of the theoretical net information rate is shown in Fig. 2(d). Using Eq. (4) Bob can post-select points about which his mutual information with Alice is greater than Eve's maximum accessible information. Applying this post-selection procedure Alice and Bob gain an "information advantage" over Eve, reversing Eve's possible information advantage prior to post-selection [6].

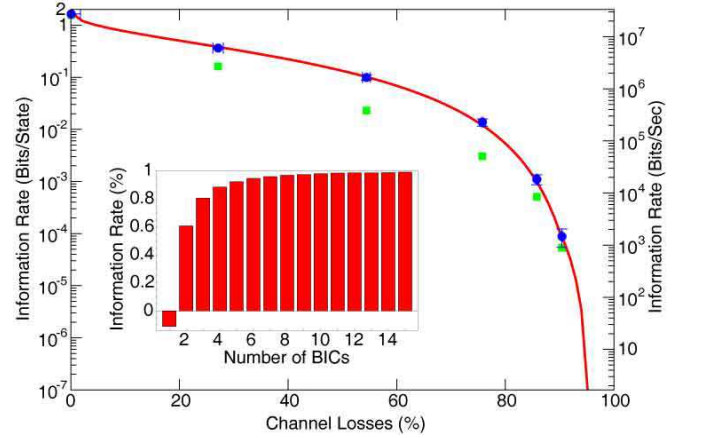


FIG. 3: Experimental secret key rate for varying quantum channel losses. Solid line: theoretical net information rate, achieved by encoding at the Shannon's capacity; Circle symbols: experimental secret key rate after post-selection; Square symbols: secret key rate after privacy amplification. (inset) Bob's mutual information with Alice (normalized to the Shannon's capacity) for increasing number of "banded information channels" (BIC) with 54% channel loss.

	90% Transmission Loss				54% Transmission Loss			
	Rate (bits/s)	$P$ Bob (%)	$P$ Eve (%)	$\Delta I$ (bits/sym)	Rate (bits/s)	$P$ Bob (%)	$P$ Eve (%)	$\Delta I$ (bits/sym)
Raw Data	$3 \times 10^7$	40	24	-0.18	$3 \times 10^7$	19	16	-0.07
Post-Selection	$6 \times 10^4$	29	30	0.01	$1 \times 10^7$	13	17	0.10
Advantage Distillation	$9 \times 10^3$	10	21	0.27	$5 \times 10^6$	5	10	0.18
Information Reconciliation	$9 \times 10^3$	$\sim 0$	8	0.40	$5 \times 10^6$	$\sim 0$	4	0.24
Privacy Amplification	$1 \times 10^3$	$\sim 0$	$\sim 50$	1.00	$4 \times 10^5$	$\sim 0$	$\sim 50$	1.00

TABLE I: Experimental results for the different stages of the QKD protocol used to distill the final secret key. Results shown for 90% and 54% transmission loss. Each procedural step shows Bob’s and Eve’s probability error rates ( $P$ ), the corresponding net information rate ( $\Delta I$  bits/symbol) and the secret key transmission rate (bits/second). Eve’s total information about the final secret key is less than one bit.

After post-selection, we proceed to distill an errorless secret key by performing an information reconciliation procedure. We take advantage of the BICs, each having differing probability error rates, by applying the reconciliation procedure iteratively to each BIC, thereby increasing the overall efficiency of the procedure. To amplify Bob’s information advantage, we apply an “ $n$ -bit repeat code” advantage distillation protocol [15], at the cost of reducing the size of the key. After advantage distillation, we apply the well known “Cascade” error reconciliation protocol [16] to correct the remaining errors. We distill a final secret key by employing a privacy amplification procedure based on universal hashing functions [17]. Eve’s resulting information about the final secret key for each BIC is  $2^{-s}/\ln 2$  bits, where  $s$  is a security factor. We decrease Eve’s total information about the final secret key (summed over all BICs and both quadratures) to less than one bit by discarding an additional  $s = 5$  bits per BIC.

Table 1 shows the experimental results for the different processes used to distill a final secret key. In the case of 90% transmission loss, Eve’s probability error rate in the raw data is lower than Bob’s error rate with a corresponding negative information rate of  $\Delta I = -0.18$  bits/symbol. Using post-selection Alice and Bob get a slight information advantage over Eve ( $\Delta I = 0.01$  bits/symbol), which is further enhanced through advantage distillation. The cost of these processes is a reduction in the size of the secret key, as can be seen in the bit-rate column in Table 1. Alice and Bob reconcile an errorless string using the Cascade protocol, which leaks additional information to Eve, decreasing her probability of error to  $\sim 8\%$ . Privacy amplification is performed to reduce Eve’s knowledge of the final key to less than 1 bit in total. To ensure that the security of our protocol is maintained during each of the processing stages, we attribute Eve, in each of these stages, a level of information that is above the maximum theoretical information that she could have obtained.

Figure 3 shows the secret key rate of our QKD protocol as a function of transmission loss. For a lossless quantum channel we achieve a final secret key rate of  $\sim 25$  Mbits/s. For transmission losses of 90%, we are still able to generate a final

secret key at a rate of  $\sim 1$  kbits/s out of only 17 MHz of our broadband spectrum, which represents a major improvement over previous protocols. The solid line in Fig. 3 gives the theoretical curve for transmitting information at the Shannon’s limit. For all transmission losses, the experimental secret key rate after post-selection is at this limit. The final secret key rate is less than the Shannon’s capacity as the information reconciliation procedure discloses more error correction information than Shannon’s equivocation limit stipulates [14]. The size of the final secret key that can be extracted after privacy amplification is calculated using Eve’s R enyi entropy (Fig. 3), which is always a lower bound on her Shannon entropy.

In conclusion, we have implemented an end-to-end coherent state QKD protocol for channel losses up to 90% by using weak sideband modulation techniques and simultaneously measuring the amplitude and phase quadratures of the electromagnetic field. This leads to high secret key rates. In our analysis we only consider 17 MHz of the sideband frequency spectrum. Extending this analysis to a much larger frequency bandwidth will enable orders of magnitude increase in the rate of secret key generation. Our system is not hampered by the technical difficulties of production and detection of single photon states that constrain discrete variable QKD protocols. We show that our protocol is secure against an optimal eavesdropping attack, and in our analysis we always assume maximal estimates of Eve’s information. The QKD scheme demonstrated provides a viable platform for the development of real-world cryptographic applications over local area networks, or city-wide networks.

We thank W. P. Bowen, T. J. Williams and D. Pulford for useful discussions. Supported by the Australian Research Council and the Australian Department of Defence.

- 
- [1] N. Gisin, G. Ribordy, W. Tittel, H. Zbinden, *Rev. Mod. Phys.* **74**, 145 (2002).
  - [2] S. L. Braunstein, A. K. Pati, *Quantum Information Theory with Continuous Variables* (Kluwer Academic Publisher 2003).

- [3] C. H. Bennett, G. Brassard, *Proceedings IEEE International Conference on Computers, Systems and Signal Proceedings (Bangalore)* (IEEE, New York, 1984), pp. 175-179.
- [4] T. C. Ralph, *Phys. Rev. A*, **61**, 010302(R) (2000).
- [5] F. Grosshans, P. Grangier, *Phys. Rev. Lett.*, **88**, 057902 (2002).
- [6] Ch. Silberhorn, T. C. Ralph, N. Lutkenhaus, G. Leuchs, *Phys. Rev. Lett.*, **89**, 167901 (2002).
- [7] F. Grosshans *et al.*, *Nature*, **421**, 238 (2003).
- [8] C. Weedbrook *et al.*, *Phys. Rev. Lett.*, **93**, 170504 (2004).
- [9] S. Lorenz, N. Korolkova, G. Leuchs, *Appl. Phys. B.*, **79**, 273 (2004).
- [10] M. Hillery, *Phys. Rev. A*, **61**, 022309 (2000); N. J. Cerf, M. Levy, G. Van Assche, *Phys. Rev. A*, **63**, 052311 (2001); D. Gottesman, J. Preskill, *Phys. Rev. A*, **63**, 022309 (2001); Ch. Silberhorn, N. Korolkova, G. Leuchs *Phys. Rev. Lett.*, **88**, 167902 (2002); K. Bencheikh, T. Symul, A. Jankovic, J. A. Levenson *J. Mod. Opt.*, **48**, 1903 (2001).
- [11] Ph. Grangier, J. A. Levenson, J.-Ph. Poizat, *Nature*, **396**, 537 (1998).
- [12] M. A. Nielsen, I. L. Chuang, in *Quantum Computation and Quantum Information*, (Cambridge University Press, Cambridge, 2000).
- [13] L. B. Levitin, in *Quantum Communications and Measurements*, edited by V.P.Belavkin, O.Hirota, and R.L. Hudson (Plenum Press, New York, 1995), pp. 439-448; C. A. Fuchs, *Proceedings of the Fourth International Conference on Quantum Communication, Measuring and Computing, 1998*, (Kluwer Academic, New York, 2000), pp. 11-16.
- [14] C. E. Shannon, *Bell Syst. Tech. J.*, **27**, 623 (1948).
- [15] U. M. Maurer, *IEEE Trans. Inf. Theory*, **39**, 733 (1993).
- [16] G. Brassard, L. Salvail, *Advances in Cryptology-Eurocrypt'93*, (Springer-Verlag, New York, 1993), pp. 411-423.
- [17] C. H. Bennett, G. Brassard, C. Crepeau, U. M. Maurer, *IEEE Trans. Inf. Theory*, **41**, 1915 (1995); C. Cachin, U. M. Maurer, *J. Cryptology*, **10**, 97 (1997).